NASA TECHNICAL MEMORANDUM

NASA TM X-1282

NASA TM X-1282

ANALOG COMPUTER STUDY OF TEMPERATURE GRADIENTS OF A SOLAR COLLECTOR IN ECLIPTIC EARTH ORBIT

by Ronald L. Thomas

Lewis Research Center

Cleveland, Ohio

NATIONAL AERONAUTICS AND SPACE ADMINISTRATION • WASHINGTON, D. C. • SEPTEMBER 1966

NASA TM X-1282

ANALOG COMPUTER STUDY OF TEMPERATURE GRADIENTS OF A SOLAR COLLECTOR IN ECLIPTIC EARTH ORBIT

By Ronald L. Thomas

Lewis Research Center
Cleveland, Ohio

NATIONAL AERONAUTICS AND SPACE ADMINISTRATION

For sale by the Clearinghouse for Federal Scientific and Technical Information
Springfield, Virginia 22151 – Price $2.00

ANALOG COMPUTER STUDY OF TEMPERATURE GRADIENTS OF A SOLAR COLLECTOR IN ECLIPTIC EARTH ORBIT

by Ronald L. Thomas

Lewis Research Center

SUMMARY

Temperature gradients required for analysis of surface distortions of a 20-foot-diameter magnesium solar collector operating in a 300-nautical-mile ecliptic Earth orbit were determined by means of analog computer simulation. The collector design studied had radial and circumferential supporting ribs on the back surface. Temperature gradients were determined for the surface sections formed by these ribs; in addition, temperature gradients radially across the collector were determined. The report discusses the computer program used and the information obtained; it does not treat the use of this information for surface distortion analysis.

For the surface section study, the heat inputs were functions of orbit position and were considered uniform across the section. Six surface conditions and five surface section sizes and rib depths were studied. Of the six surface conditions studied, the polished metal front with insulated back resulted in the lowest maximum temperature gradients. The temperature gradients across the surface sections and from sections to adjacent ribs were found to be nearly constant (0.2° and 0.7° F/in., respectively) for different surface section sizes with the same rib depth. The gradients were found to vary primarily with rib depth.

For the radial temperature gradient study, the heat inputs to the collector were functions of position on the collector as well as collector position in orbit. Temperature distributions were determined along two adjacent ribs of different thicknesses. Results indicate typical radial temperature gradients of approximately 0.27° and 0.17° F per inch for the 0.120- and 0.380-inch-deep radial ribs, respectively. Comparison of the two radial studies indicates that the maximum circumferential gradient could reach 0.925° F per inch between inner mirror sections (neglecting conduction).

INTRODUCTION

Some technical problems related to the feasibility of developing a solar Brayton space-power system are being investigated at Lewis. Such a system uses a parabolic solar collector (mirror) for reflecting the rays of the Sun into a heat-storage - heat-exchanger component known as an absorber. While exposed to the Sun, the absorber transfers heat to a working gas and also melts a heat-storage medium, such as lithium fluoride. The melted lithium fluoride supplies latent heat to the gas during the shade portion of the orbit. The hot gas is used to drive a turboalternator that generates electrical power, which is the system output. The closed Brayton cycle also includes a recuperator, radiator, and turbocompressor.

The structural design of the solar collector is being investigated. Previous work in this area is reported in references 1 and 2. The collector, of course, must be low in weight and high in efficiency. For high efficiency, a surface with good reflectivity and with a contour closely approaching a true parabola is necessary. The problem of preserving the contour of a fixed geometry collector during launch and maneuver loads dictates the general structural design. A design selected for further study uses radial and circumferential supporting ribs as an integral part of the back surface of the parabolic mirror, thus forming a waffle-type structure. Several sizes of waffle patterns are being considered along with several combinations of front and back surface conditions, for example, front coated with back insulated, or front polished and back coated, etc. With the waffle design, however, a potential problem of surface distortion in Earth orbit exists because of temperature gradients. This problem prompted the study of the temperature gradients reported herein. This study determines the particular waffle-type structure and surface conditions that provide minimum temperature gradients. This best design could be analyzed in detail for surface distortions. This report, however, covers the temperature gradient study only.

The study was conducted on an analog computer using a many-lump solution of the heat-transfer equations. For the study, a 20-foot-diameter collector orbiting the Earth in a 300-nautical-mile ecliptic path was assumed. The collector material considered was magnesium. If the material were aluminum, the temperature gradients would be less, since the conductivity of aluminum is more than twice that of the magnesium alloy considered. The maximum temperature gradients are presented for the surface sections formed by the ribs. The temperature gradients determined radially across the collector for two thicknesses of radial ribs are also presented. Circumferential temperature gradients around the collector are estimated by comparing the temperature distributions obtained for the two radial ribs.

SYMBOLS

A	surface area, sq ft
A_x	cross-sectional area, sq ft
C	specific heat, Btu/(lb)(^oR)
k	conductivity, Btu/(hr)(ft)(^oR)
L	conduction length, ft
Q	heat input, Btu/(hr)(sq ft)
T	temperature, ^oR
t	thickness, ft
W	weight, lb
α	absorptivity
Δ	designated perturbation quantities
ϵ	emissivity
σ	Stefan-Boltzmann constant, Btu/(hr)(sq ft)($^oR^4$)

Subscripts:

a, b, c, d	column designation for surface section study
o	approximate average
r	rib
rs	radial segment
s	sheet
ss	surface section
1, 2, 3, 4, 5, 6, 7	row designation for surface section study
1 to 18	used for lump designation in radial study

METHOD OF ANALYSIS

Surface Section Study

Mathematical model. - For this study, the surface sections formed by the ribs were assumed to be square. The geometry of the surface section and supporting ribs studied

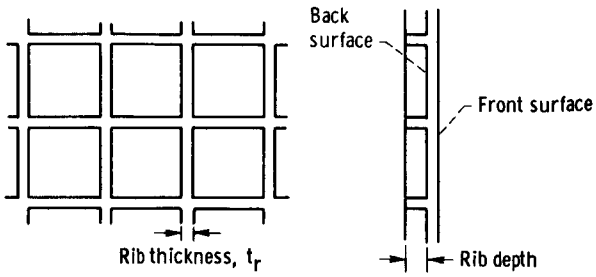

(a) Surface sections.

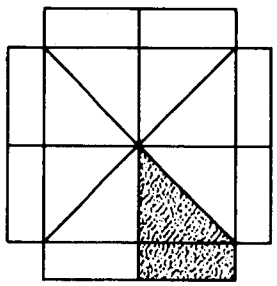

(b) Division of surface sections and ribs into eight symmetrical parts (ribs spread out).

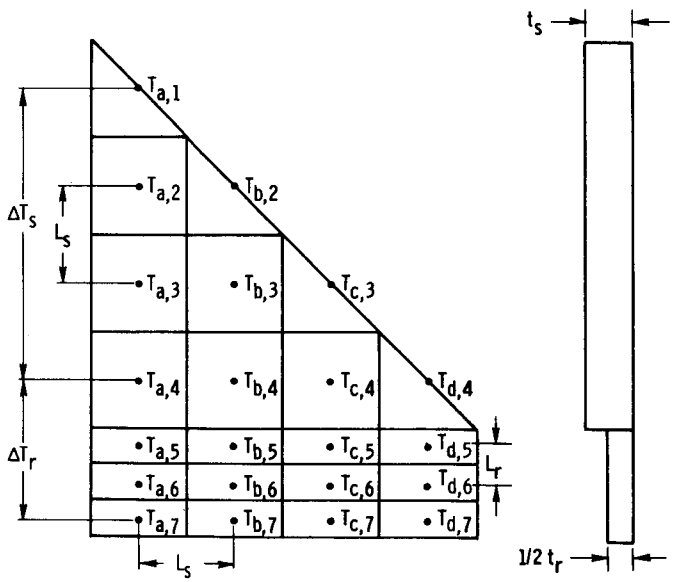

(c) Distribution of nodes in surface section.

Figure 1. - Surface-section configuration used.

is shown in figure 1(a). The temperature distribution within a given square was analyzed. Since one surface section represents a small part of the total surface of the mirror, all heat was assumed to enter the surface section uniformly. For such a periodic structure, no heat flows across lines about which the pattern is symmetric. Three such lines of symmetry are (1) the centerline of the ribs, (2) the line through the center of each square and parallel to the ribs, and (3) the diagonal line through opposite corners of a given square. Such adiabatic boundaries simplify the analysis because a surface section within such an adiabatic boundary may be considered isolated from its surroundings. For analysis of the temperature distribution within a given square, a surface section was defined by the three boundaries cited previously and is shown as the shaded portion in figure 1(b). Because the thicknesses of the ribs and front surface are small in relation to the other dimensions of a given square, the half-ribs of a given surface section were analyzed as if folded into the plane of the front surface (fig. 1(b)). Each such surface section was then divided into 22 lumps with a temperature node for each lump (fig. 1(c)).

The section sizes considered were (in inches) 6 by 6 by 1, 8 by 8 by 1, 6 by 6 by 4, 4 by 4 by 1, and 2 by 2 by 1/2. For each size, the first two digits represent the surface section

length and width and the third digit represents the rib depth. The front surface and rib thicknesses were 0.050 inch for all studies except for the 0.125-inch rib thickness of the 6 by 6 by 4 size. For the various geometries, the six surface conditions studied with their respective absorptivities and emissivities are listed in table I.

TABLE I. - COLLECTOR SURFACE CONDITIONS

Case	Front surface				Back surface			
	Condition	Absorptivity		Emissivity	Condition	Absorptivity		Emissivity
		Solar	Thermal			Solar	Thermal	
I	Silicon oxide coating	0.10	0.30	0.30	White radiative coating	0.25	0.80	0.80
II	Polished front	.10	.05	.05	White radiative coating	.25	.80	.80
III	Polished front	.10	.05	.05	Insulated	0	0	0
IV	Silicon oxide coating	.10	.30	.30	Insulated	0	0	0
V	Silicon oxide coating	.10	.30	.30	Plain metal	.10	.20	.20
VI	Polished front	.10	.05	.05	Plain metal	.10	.20	.20

To determine the node temperatures of a surface section and supporting ribs, heat-balance equations were written for each lump. For 22 lumps, this required the solution of 22 simultaneous equations. The equation for a typical node temperature $T_{b,4}$ (fig. 1(c)) is

$$W_{b,4} C\dot{T}_{b,4} = QA_{b,4} + kt_s(T_{b,3} - T_{b,4}) + kt_s(T_{a,4} - T_{b,4}) + kt_s(T_{c,4} - T_{b,4}) + \frac{kt_r L_s}{L_s + L_r}(T_{b,5} - T_{b,4}) - \epsilon\sigma A_{b,4} T_{b,4}^4 \qquad (1)$$

In order to determine accurately the small temperature differences between nodes, equation (1) was rewritten expressing node temperature as the sum of a base temperature T_o and a temperature perturbation $\Delta T_{b,4}$. The approximate average temperature of the surface and rib was used as the base temperature T_o.

$$T_{b,4} = T_o + \Delta T_{b,4} \tag{2}$$

$$\dot{T}_{b,4} = \dot{T}_o + \Delta\dot{T}_{b,4} \tag{3}$$

$$T_{b,4}^4 = (T_o + \Delta T_{b,4})^4 = T_o^4 + 4T_o^3\,\Delta T_{b,4} + 6T_o^2\,\Delta T_{b,4}^2 + 4T_o\,\Delta T_{b,4}^3 + \Delta T_{b,4}^4 \tag{4}$$

If the base temperature T_o is 500^o R and the perturbation $\Delta T_{b,4}$ is 10^o R (maximum expected), the second term on the right side of equation (4) is 8 percent of the first term T_o^4 and the third term on the right side is only 0.24 percent of the first term. Therefore, only the first two terms were retained:

$$T_{b,4}^4 \cong T_o^4 + 4T_o^3\,\Delta T_{b,4} \tag{5}$$

With the use of equations (2), (3), and (5), equation (1) can be written as

$$W_{b,4}C\,\Delta\dot{T}_{b,4} = -W_{b,4}C\,\Delta\dot{T}_o + QA_{b,4} + kt_s(\Delta T_{b,3} - \Delta T_{b,4}) + kt_s(\Delta T_{a,4} - \Delta T_{b,4})$$

$$+ kt_s(\Delta T_{c,4} - \Delta T_{b,4}) + \frac{kL_st_r}{L_s + L_r}(\Delta T_{b,5} - \Delta T_{b,4}) - \epsilon\sigma A_{b,4}(T_o^4 + 4T_o^3\,\Delta T_{b,4}) \tag{6}$$

The coefficients of the conductance terms in equation (6) were obtained by multiplying the metal conductivity k by the cross-sectional area between nodes and dividing by conduction length between nodes. For adjacent surface and rib nodes, a discontinuity of cross-sectional areas exists; the smaller cross-sectional area was used.

Heat input or output for the rib nodes was assumed by conduction only. Therefore, for rib nodes such as node $T_{a,7}$ (fig. 1(c)), equation (6) reduces to

$$W_{a,7}C\,\Delta\dot{T}_{a,7} = -W_{a,7}C\dot{T}_o + \frac{kL_rt_r}{2L_s}(\Delta T_{b,7} - \Delta T_{a,7}) + \frac{kL_st_r}{2L_r}(\Delta T_{a,6} - \Delta T_{a,7}) \tag{7}$$

In equation (7) only two conduction terms for node $T_{a,7}$ exist because of the symmetry of the surface section subdivisions. The temperature to the left of node $T_{a,7}$ (fig. 1(c)) would be equal to $T_{a,7}$ and, therefore, no heat would flow between these two nodes.

The perturbation method requires one additional equation, representing the whole sheet and rib section, for computing the approximate average temperature:

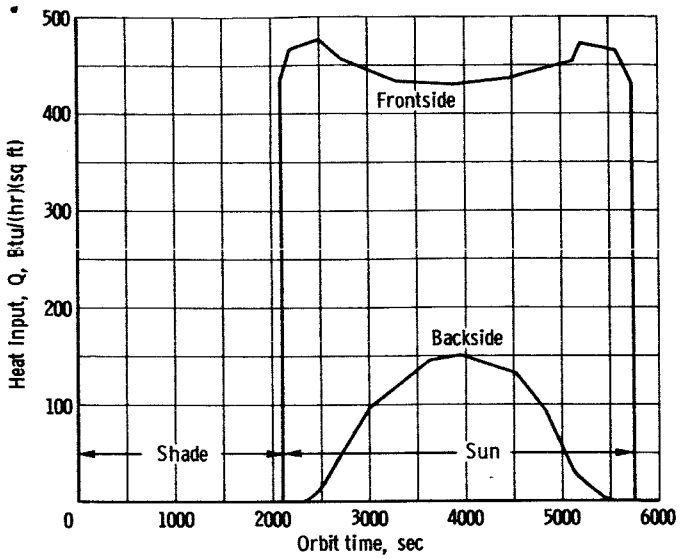

Figure 2. - Incident solar radiation to collector including effect of Earth's albedo.

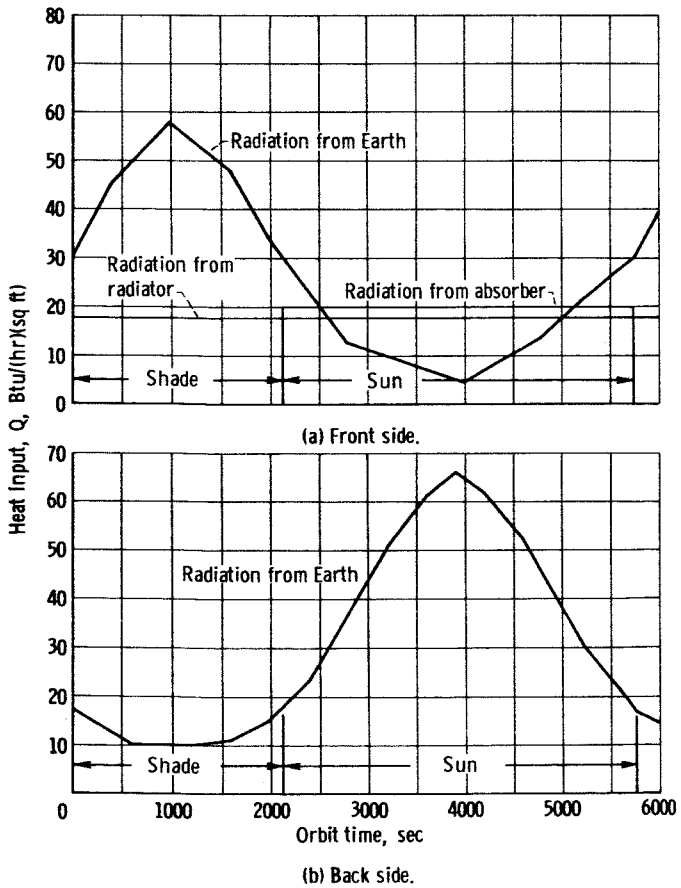

Figure 3. - Incident thermal radiation to collector.

$$W_{ss}C\dot{T}_o = QA_{ss} - \epsilon\sigma A_{ss}T_o^4 \qquad (8)$$

Computer techniques. - The heat input Q in equations (6) and (8) represents the total heat input to the front and back of the collector and is the sum of incident solar and thermal radiation, each multiplied by the pertinent absorptivity. Obviously, for a Sun-to-shade orbit, the heat input to the collector will vary with position in orbit. The assumed variation of incident solar radiation to the front and back side of the collector is shown in figure 2, with orbit time used to indicate orbit position. Incident solar radiation to the front side represents the largest heat source to the collector; however, 90 percent is reflected because the solar absorptivity is only 0.10 for all the front surfaces studied (table I). From figure 2, this solar radiation is zero during the shade period (0 to 2100 sec) and reaches a maximum of 476 Btu per hour per square foot during the Sun period of the orbit (2100 to 5700 sec). A variation of 40 Btu per hour per square foot during the Sun period is caused by the solar energy reflected from the Earth (Earth albedo) that hits the front surface of the collector.

The incident solar radiation to the back side of the collector is also shown as a function of orbit time in figure 2. Again, this is obviously zero during the shade period of the orbit and peaks halfway through the Sun period of the

orbit. The maximum of 150 Btu per hour per square foot is about one-third that of the incident solar radiation to the front of the mirror.

The variation of incident thermal radiation to the front of the collector with orbit time is shown in figure 3(a). The radiation from the Earth, the radiator, and the absorber cavity are shown separately. The Earth thermal radiation varies from 58 to 4.5 Btu per hour per square foot with the maximum and minimum occurring approximately halfway into the shade period and halfway into the Sun period, respectively. The maximum and minimum occur because the front of the collector is facing the Earth during the shade period but is facing away from the Earth during the Sun period. The radiation from the absorber cavity is zero during the shade period because the absorber cavity would presumably be covered during this period of the orbit.

The final heat input represents incident thermal radiation to the back side of the collector (fig. 3(b)). Comparison of this figure with figure 3(a) shows that the maximums (and minimums) occur at diametrically opposite points in the orbit.

For the simulation, the curves of figures 2 and 3 were programed on an analog computer by means of diode function generators. The input to these function generators was orbit time. An orbit timer was programed on the computer by using the diagram shown in figure 4. This timer circuit provided a means of running repeated orbits (see fig. 5). The simulation was time-scaled by a factor of 100; therefore, 5700 seconds of orbit time were covered in 57 seconds of computer time.

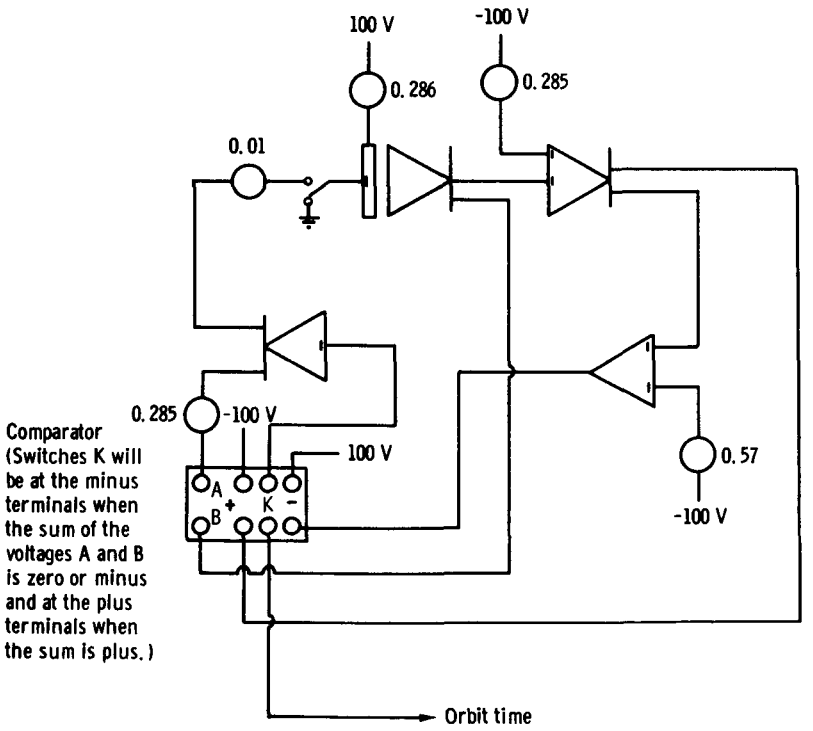

Figure 4. - Circuit for periodic orbit time.

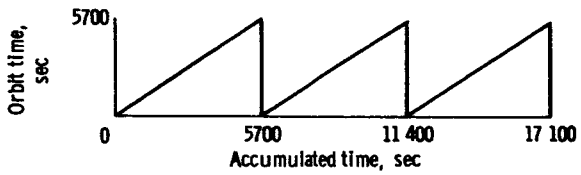

Figure 5. - Diagram of consecutive orbits.

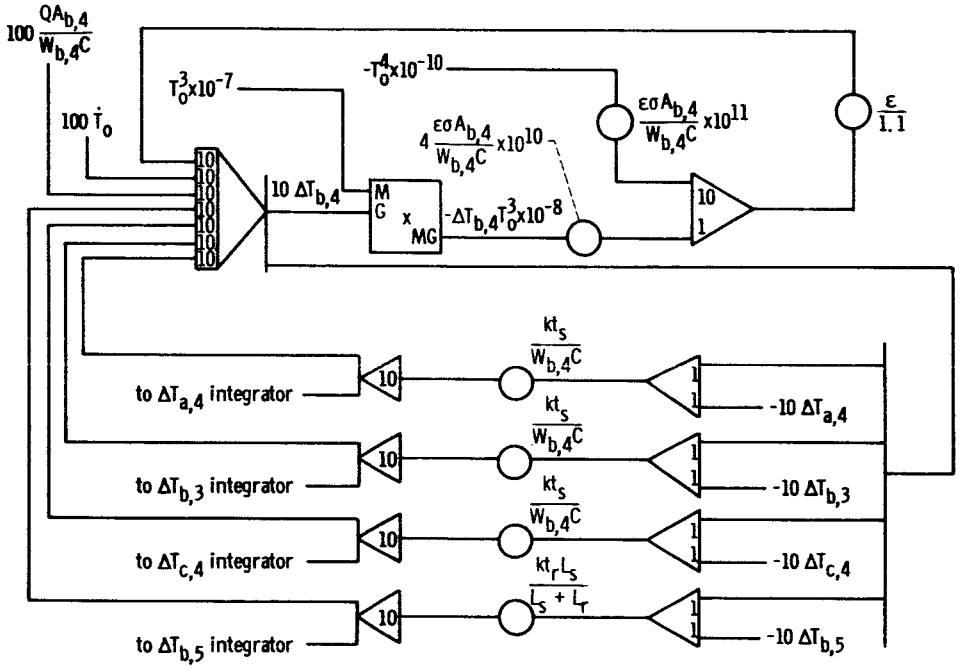

(a) Individual lump solution ($\Delta T_{b,4}$).

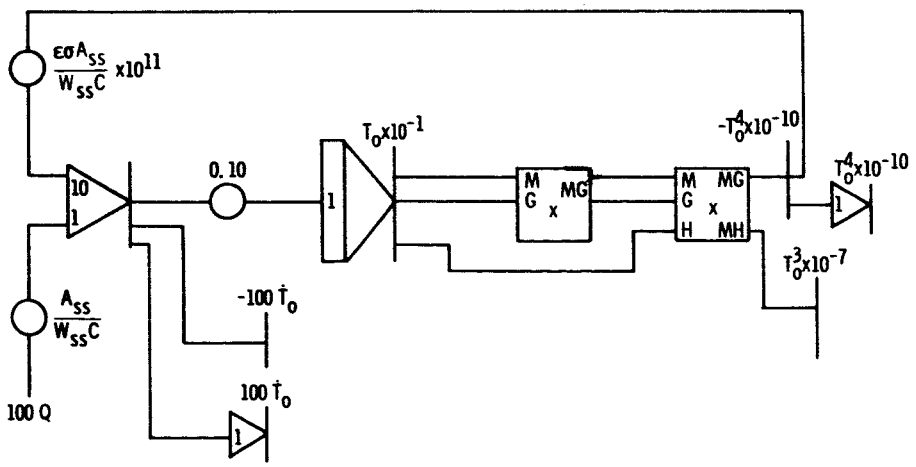

(b) Approximate average temperature of whole section.

Figure 6. - Analog computer diagrams. Time scale factor, 100.

The 23 equations discussed previously were programed on the computer for simultaneous solution of each node perturbation temperature and for T_o, the approximate average temperature of the whole section. Analog computer diagrams are shown in figure 6.

After the equations were programed on the analog computer, a dynamic check was made to make certain that the program was operating correctly. First, the sheet section was isolated from the rib section. Each node in the sheet section was then identical and each node temperature should vary in exactly the same manner with heat input. A similar test was used to check the rib section nodes with the mean temperature T_o as an artificial heat input.

Radial Study

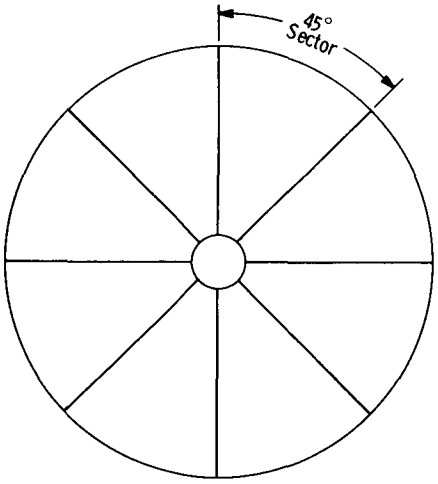

Figure 7. - Collector consisting of eight 45° sectors.

Mathematical study. - For this study, the collector is assumed to consist of eight 45° sectors formed by 0.380-inch-thick radial ribs (fig. 7). A pattern of thinner radial and circumferential ribs was also assumed to exist within each of the 45° sectors. Two studies were made to estimate the radial temperature distribution. The first was for a 15° sector located about a thin radial rib through the center of a 45° sector, and the second study was for a 15° sector located about one of the thicker radial ribs forming the boundary between two 45° sectors. The 15° sector model used for the thin-rib study was identical to the thick-rib study, except that the central rib was 0.120 inch thick and 1.5 inches deep (fig. 8(a)) compared with the thick rib that was 0.380 inch thick and 1.0 inch deep (fig. 8(b)). The rib pattern shown in figure 8 is illustrative of what may be used for structural reasons.

For the analysis of the radial temperature gradient, a temperature node was assumed at the center of each of the 18 lumps shown in figure 8. Heat balance equations were written for each of the 18 lumps to obtain the node temperatures, the temperature differences between each node, and the approximate average temperature T_o of the 15° sector. For example, the heat balance equation for lump 4 is

$$W_4 C\,\Delta\dot{T}_4 = -W_4 C\dot{T}_o + QA_4 + \frac{kA_{x,4,3}}{L_{4,3}}(\Delta T_3 - \Delta T_4) + \frac{kA_{x,4,5}}{L_{4,5}}(\Delta T_5 - \Delta T_4) - \epsilon\sigma A_4\left(T_o^4 + 4T_o^3\,\Delta T_4\right) \qquad (9)$$

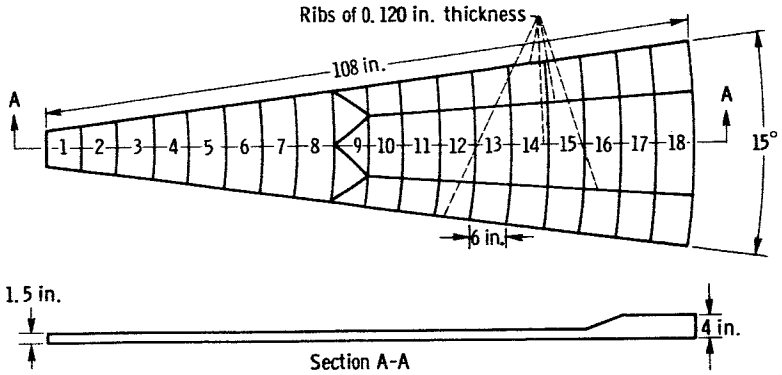

Dimensions of 0.120-inch-thick radial ribs are shown in section A-A; all other ribs are 1.0 inch deep and 0.05 inch thick except at lump 18, where they are 4.0 inches deep.

(a) Study of radial rib of 0.120 inch thickness.

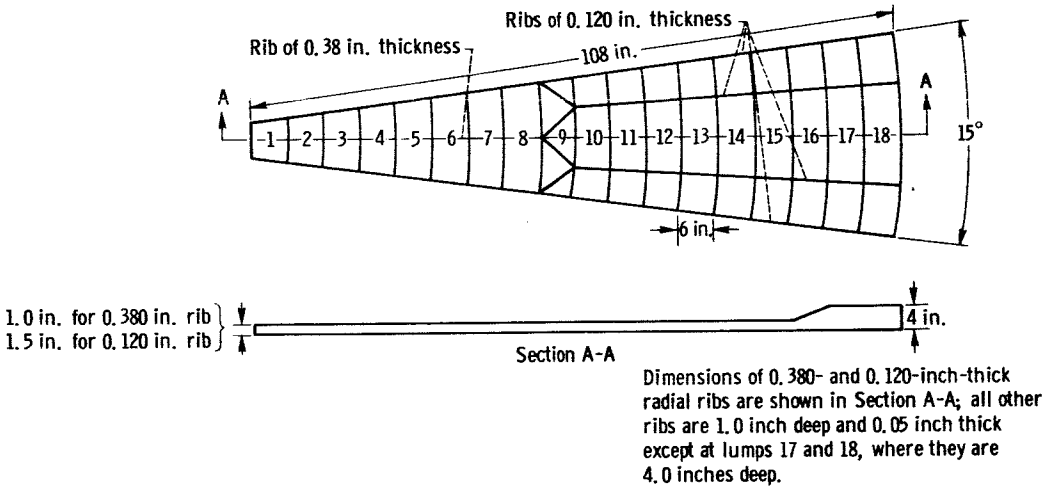

Dimensions of 0.380- and 0.120-inch-thick radial ribs are shown in Section A-A; all other ribs are 1.0 inch deep and 0.05 inch thick except at lumps 17 and 18, where they are 4.0 inches deep.

(b) Study of radial rib of 0.380 inch thickness.

Figure 8. - 15° Sectors of collector used for radial-rib study.

where A_4 represents surface area of lump 4, $A_{x,4,3}$ is the cross-sectional area between lumps 4 and 3, and $L_{4,3}$ is the conduction length between nodes 4 and 3.

The approximate average temperature T_o is obtained from

$$W_{rs} C \dot{T}_o = Q A_{rs} - \epsilon \sigma A_{rs} T_o^4 \tag{10}$$

For this study, only radial heat conduction was considered. However, by comparing the results of the two radial studies, it was possible to make conservative estimates of the circumferential gradients.

For both of the radial studies, it was assumed that the front surface of the collector was coated with silicon oxide and that the back surface was insulated (case IV, table I,

TABLE II. - SOLAR, ABSORBER, AND RADIATOR HEAT INPUTS TO FRONT SURFACE OF COLLECTOR FOR RADIAL STUDY

Radial lump[a]	Heat input, Btu/(hr)(sq ft)		
	Solar (Sun phase only)	Absorber (Sun phase only)	Radiator (Entire orbit)
1	428	23	18
2	427	23	
3	425	22	
4	424	21	
5	420	20	
6	418	19	
7	415	18	
8	412	17	
9	408	16	
10	404	15	
11	400	14	
12	396	13	
13	392	12	
14	388	11	
15	383	10	
16	378	9	
17	374	8	
18	369	7	

[a]See fig. 8(b).

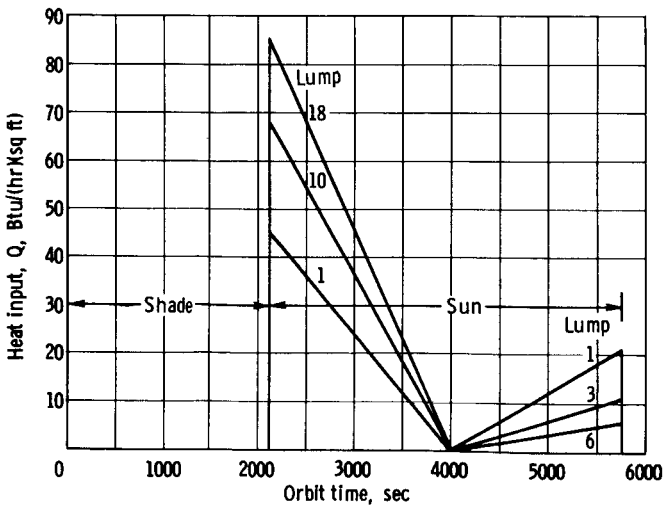

Figure 9. - Earth albedo for several lumps of collector model.

p. 5). The surface section sizes for the radial study correspond approximately to the 6 by 6 by 1 inch size investigated in the Surface Section Study.

Computer techniques. - The heat input term Q in equations (9) and (10) is a function of position on the collector as well as collector position in orbit, and it represents the sum of the heat inputs to the front surface of the collector, each heat input multiplied by its respective absorptivity. The heat inputs to the back surface were neglected because the back of the collector was assumed to be insulated. The incident solar radiation and the absorber and radiator thermal radiation for each lump is shown in table II. For a given lump, the solar and absorber radiations are constant during the Sun period of orbit and zero during the shade period. The radiator thermal radiation is constant at 18 Btu per hour per square foot for each lump throughout the Sun and shade periods of the orbit. The solar radiation is a maximum of 428 Btu per hour per square foot for lump 1 and a minimum of 369 Btu per hour per square foot for lump 18. The absorber heat input varies from 23 Btu per hour per square foot for lump 1 to 7 Btu per hour per square foot for lump 18. The thermal radiation from the Earth to the front surface of the collector was assumed to be constant from one lump to another. The input used was the same as that for the Surface Section Study, which was shown in figure 3(a) (p. 7). Solar radiation reflected from

the Earth to the front surface of the collector (Earth albedo) is shown in figure 9 as a function of orbit time. This reflected solar radiation reaches a maximum of 85 Btu per hour per square foot for the outermost lump, which is lump 18, just as the collector comes into the Sun period. With the collector halfway through the Sun period, the albedo for all lumps is zero; for the last half of the Sun period, the Earth albedo increases for the inner six lumps.

As discussed in the Surface Section Study, the heat inputs were programed on the computer to vary with orbit time. Again, a timer circuit was used and the problem was time-scaled such that orbits of 5700 seconds could be run in 57 seconds. The 18 equations for determining the node perturbation temperatures for each lump and the one equation for determining the approximate average temperature of the whole section were programed on the computer and solved simultaneously. The perturbation temperatures for each lump were determined as functions of orbit position.

RESULTS AND DISCUSSION

Surface Section Study

Rib geometry. - Studies were made of 11 combinations of surface conditions, section

TABLE III. - MAXIMUM SHEET AND RIB TEMPERATURE DIFFERENCES AND GRADIENTS DURING SUN PHASE OF 300-NAUTICAL-MILE ECLIPTIC ORBIT

Section size, in.	Case	Sheet temperature difference, ΔT_s	Ratio of sheet temperature difference to conduction length difference, $\Delta T_s/\Delta L$	Rib temperature difference, ΔT_r	Ratio of rib temperature difference to conduction length difference, $\Delta T_r/\Delta L$
6 by 6 by 1	I	0.90	0.40	1.50	1.20
6 by 6 by 1	II	1.0	.44	1.70	1.40
6 by 6 by 1	III	.50	.22	.80	.66
2 by 2 by 1/2	IV	.10	.13	.20	.37
4 by 4 by 1	IV	.35	.23	.70	.65
6 by 6 by 1	IV	.50	.22	.90	.74
8 by 8 by 1	IV	.70	.23	1.00	.75
6 by 6 by 4	IV	1.20	.53	2.40	.65
6 by 6 by 1	V	.60	.27	1.00	.83
6 by 6 by 1	VI	.55	.25	.90	.74

sizes, and rib depths to determine what combinations provide a collector with minimum temperature gradients during a 300-nautical-mile ecliptic Earth orbit. Only two temperature differences are referred to in this report for making comparisons of the results of the different studies: first, the sheet temperature difference ΔT_s, which is the temperature difference between a node near the center of the sheet and the last node in the sheet next to the rib, and second, the rib temperature difference ΔT_r, which is the temperature difference across the rib depth from the sheet node nearest the rib to the last node on the rib (see fig. 1). The maximum ΔT_s and ΔT_r temperature differences to occur during the Sun phase of an orbit for different collector surfaces and section sizes are shown in table III. These maximum temperature differences occur shortly after the mirror enters the Sun period of orbit. Time histories of surface section and rib temperature differences during three or more orbits are shown in figure 10 for all studies listed in table III. As can be seen from these figures, the maximum temperature differences during an orbit actually occurred as the collector went from Sun to shade, and were as much as 50 percent larger than those that occurred during the Sun period. These temperature differences, however, are not as important since collector distortion during shade operation will not affect the power system (providing distortion does not cause permanent set).

The computer results in table III show that the maximum temperature differences of the sheet ΔT_s increase with increased sheet size (conduction length) as expected. The sheet temperature gradients, however, are approximately 0.23° R per inch for the 4 by 4 by 1, 6 by 6 by 1, and 8 by 8 by 1 section sizes. For the 6 by 6 by 4 section, however, the sheet temperature gradient is about twice as large. This implies that rib depth is the important variable in determining the maximum sheet temperature gradient. Further evidence is given by the results for the 2 by 2 by 1/2 section, which has a maximum sheet temperature gradient of approximately one-half the value obtained for the sections with the 1-inch rib depth. Obviously, if the rib depth were reduced to zero, the sheet temperature differences would be zero for uniform heat input.

The rib temperature difference ΔT_r increased as either rib depth or sheet size increased. This result is logical because an increase in either sheet size or rib depth increases conduction length. Maximum rib temperature gradients of approximately 0.70° R per inch were obtained for the 4 by 4 by 1, 6 by 6 by 1, and 8 by 8 by 1 sections, but the gradients are reduced by one-half for the 2 by 2 by 1/2 section. Other results, however, show that the rib temperature gradient ΔT_r is not proportional to rib depth: the 6 by 6 by 4 section has a slightly lower ΔT_r than the 6 by 6 by 1 section.

Mirror surface treatment. - For the six surface combinations studied, the two with the back surface of the collector insulated resulted in the lowest sheet and rib temperature gradients (cases III and IV, table I). These temperature gradients are the lowest because the heat input to the collector is less with the back insulated, which results in

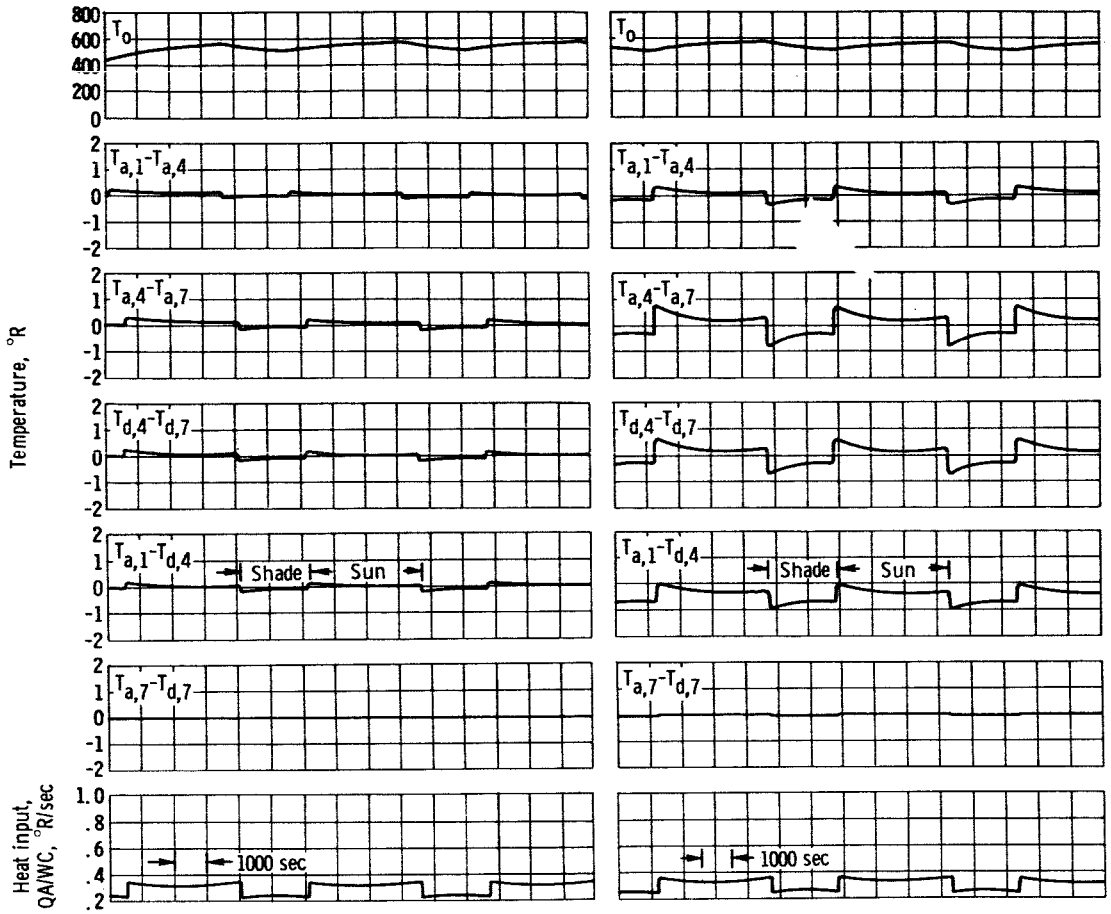

(a) Section size, 2 by 2 by 1/2 inch; case IV surface condition.

(b) 4 by 4 by 1 section with case IV surface conditions.

Figure 10. - Time histories of temperatures and heat inputs for several combinations of section size and collector surface conditions.

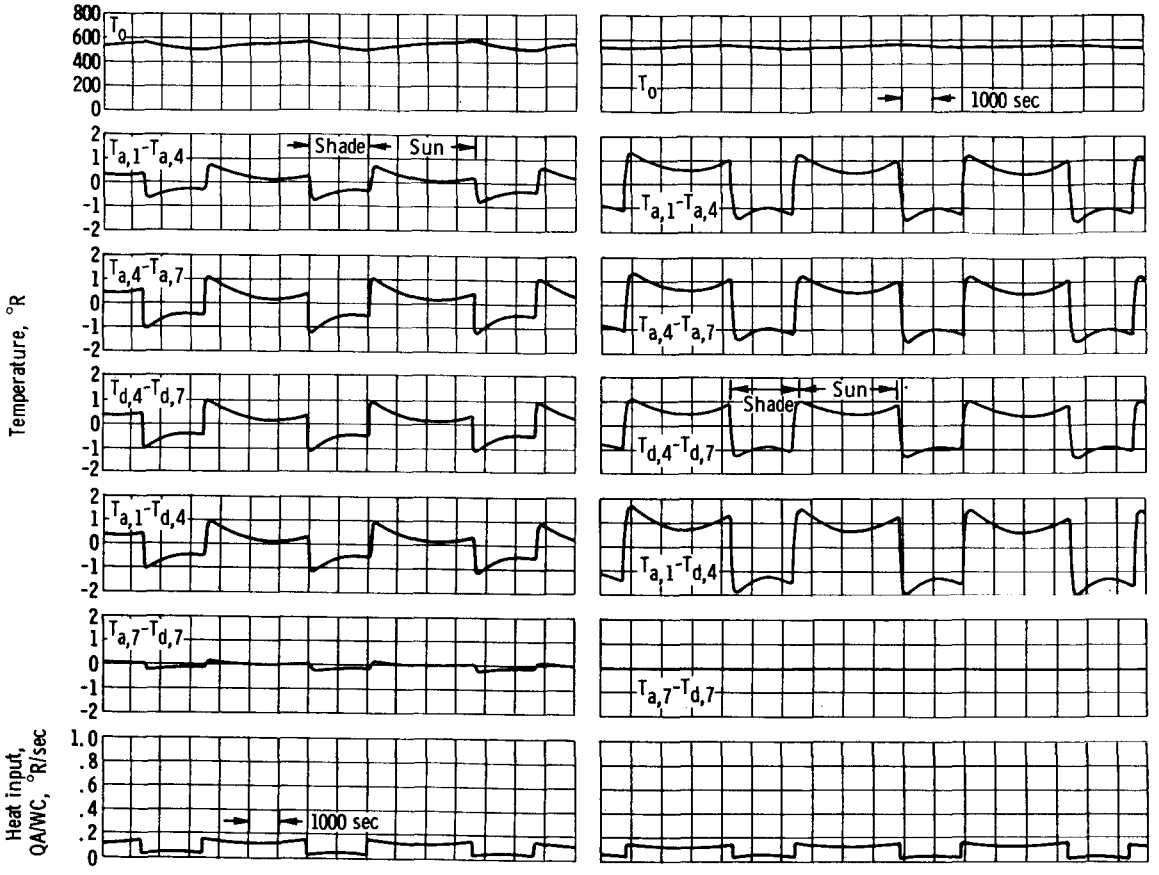

(c) 8 by 8 by 1 section with case IV surface conditions.

(d) 6 by 6 by 4 section with case IV surface conditions.

Figure 10. - Continued.

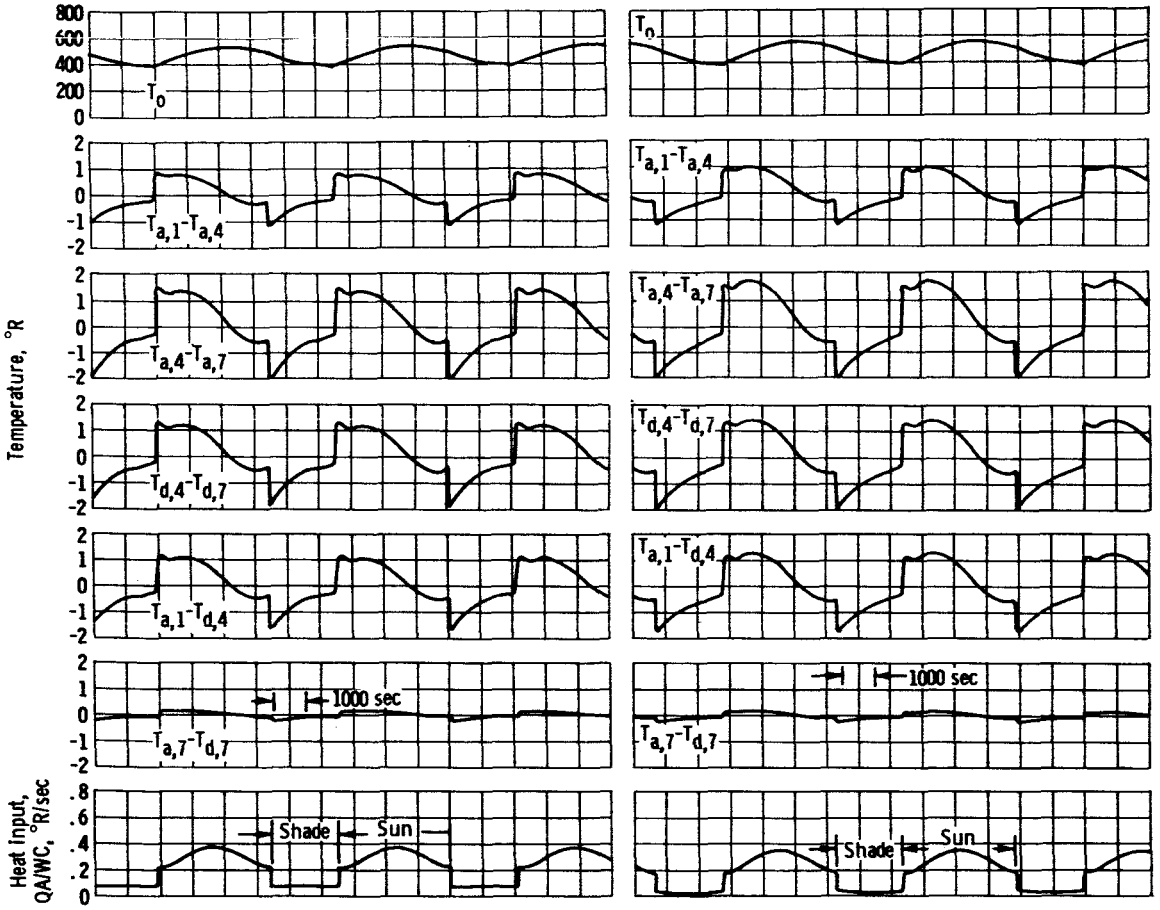

(e) 6 by 6 by 1 section with case I surface conditions.

(f) 6 by 6 by 1 section with case II surface conditions.

Figure 10. - Continued.

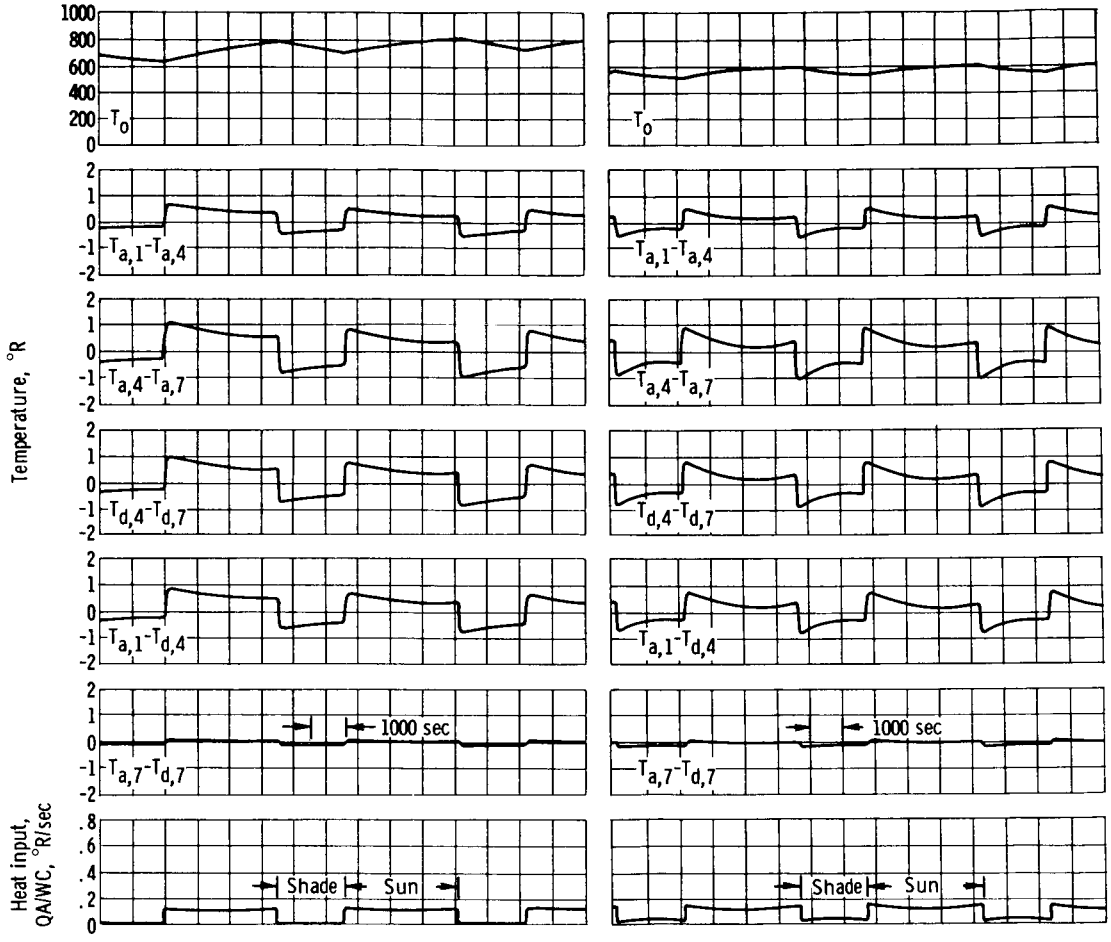

(g) 6 by 6 by 1 section with case III surface conditions.

(h) 6 by 6 by 1 section with case IV surface conditions.

Figure 10. - Continued.

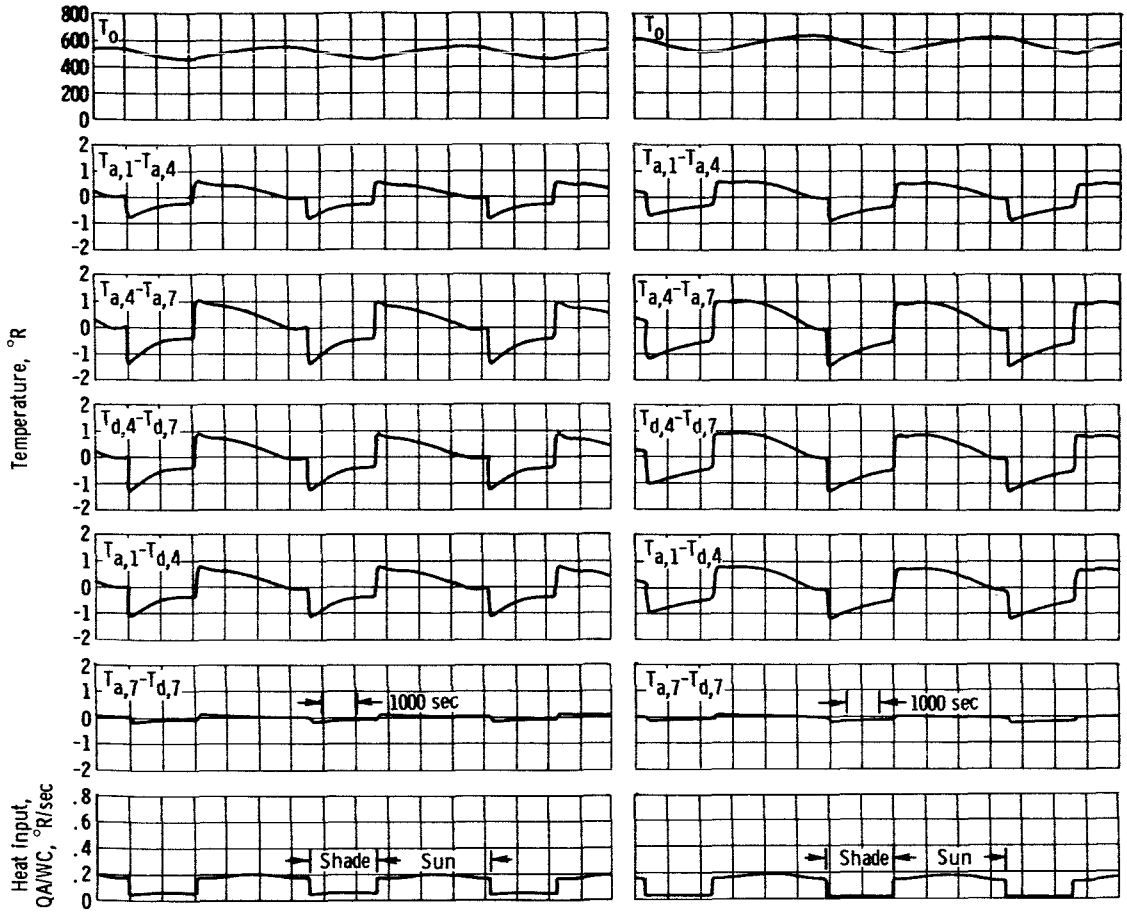

(i) 6 by 6 by 1 section with case V surface conditions.

(j) 6 by 6 by 1 section with case VI surface conditions.

Figure 10. - Concluded.

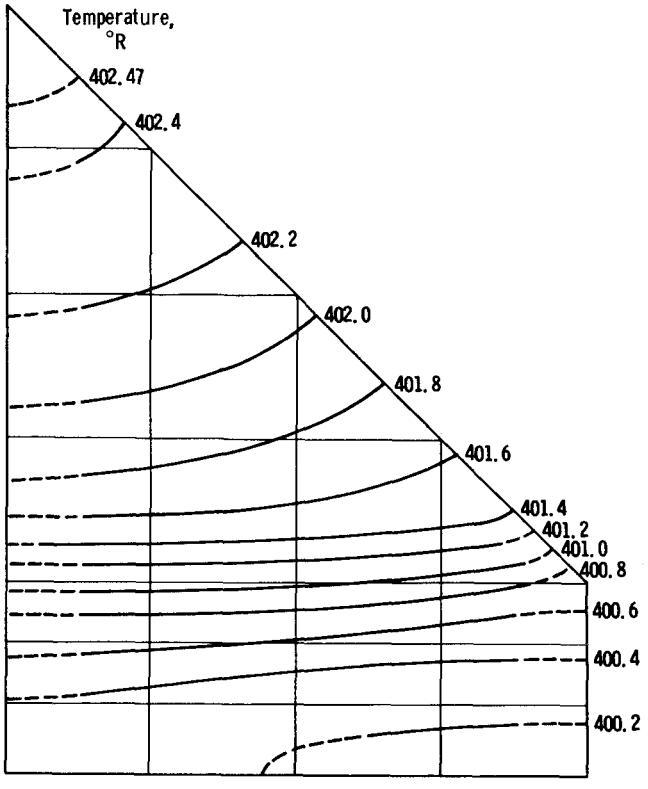

Figure 11. - Temperature distribution in 6-by-6-by-1-inch section 200 seconds after entering Sun period. Case I surface conditions.

less heat input change as the collector goes from shade to Sun. The relation between the gradients and the heat input changes can be seen in figure 10. Of the two front surface conditions studied with the back insulated, the polished metal front results in slightly lower temperature gradients than the silicon-monoxide-coated front. The polished front has a lower thermal absorptivity than the silicon-monoxide-coated front and, therefore, a smaller heat input change. The temperature distribution for the 6 by 6 by 1 section with a silicon-monoxide-coated front surface and white radiative back surface is shown in figure 11. This temperature distribution exists 200 seconds after leaving the shade.

Radial Study

As mentioned in the earlier Radial Study section, the purpose of this study was to obtain the temperature gradients of the collector along the full length of a radial rib. Two studies were made: one was for a 0.120-inch-thick rib through the center of one of the eight symmetrical 45° sectors, and the other was for a 0.380-inch-thick rib forming the boundary between two of the 45° sectors. These studies were made for a collector with a silicon-oxide-coated front surface and an insulated back surface (case IV,

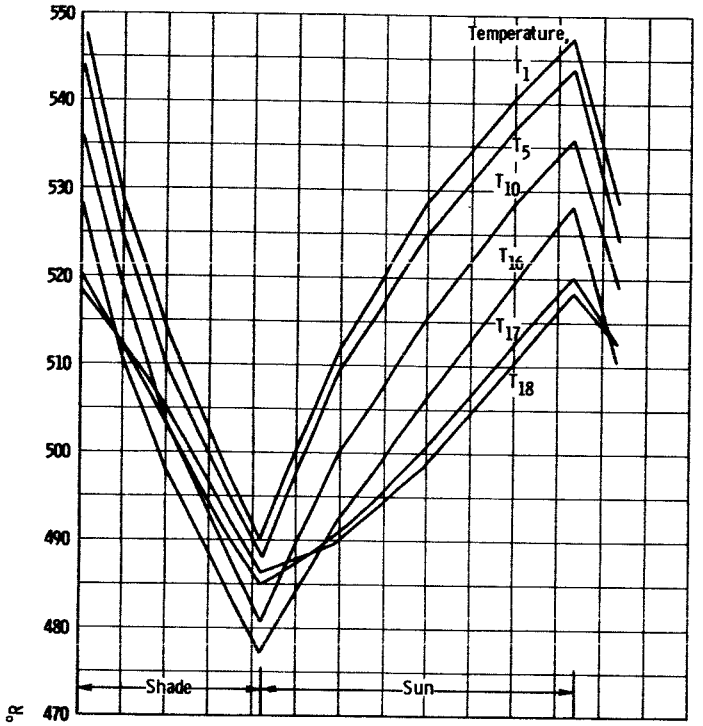

(a) Temperature variation of several lumps with orbit time for 0.120-inch-thick radial rib.

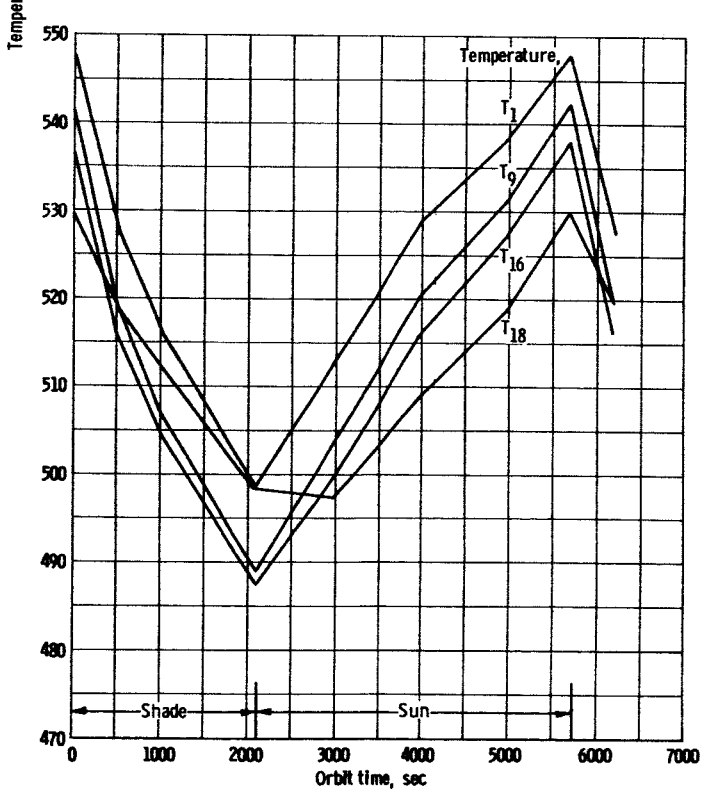

Temperature, °R

(b) Temperature variation of several lumps with orbit time for 0.380-inch-thick radial rib.

Figure 12. - Temperature distributions for radial ribs.

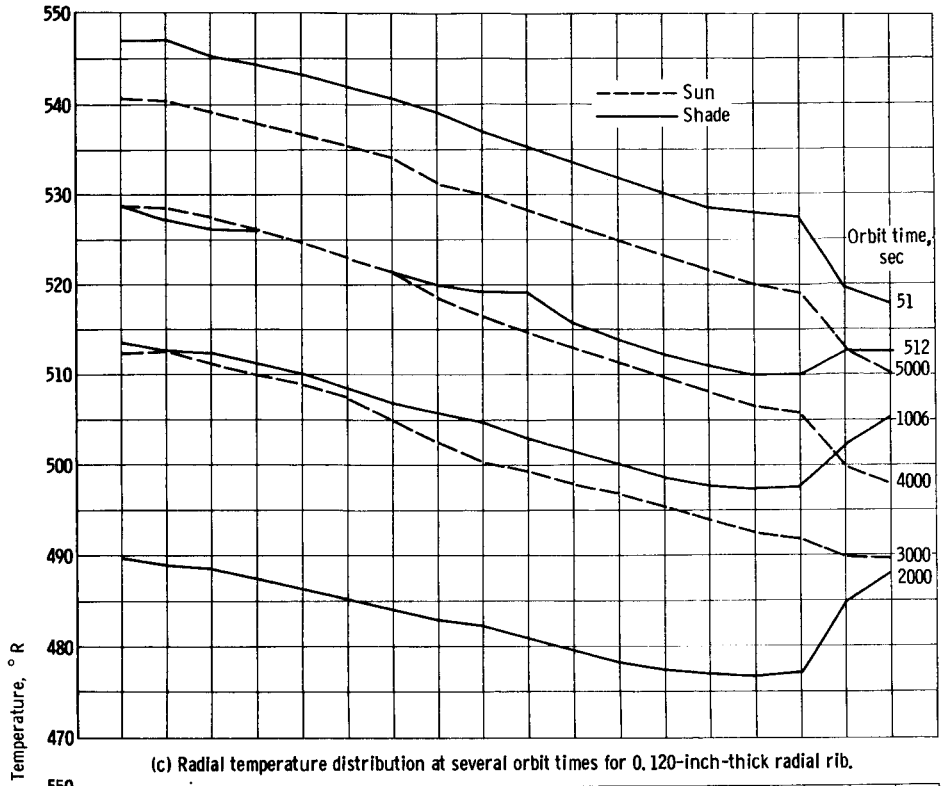

(c) Radial temperature distribution at several orbit times for 0.120-inch-thick radial rib.

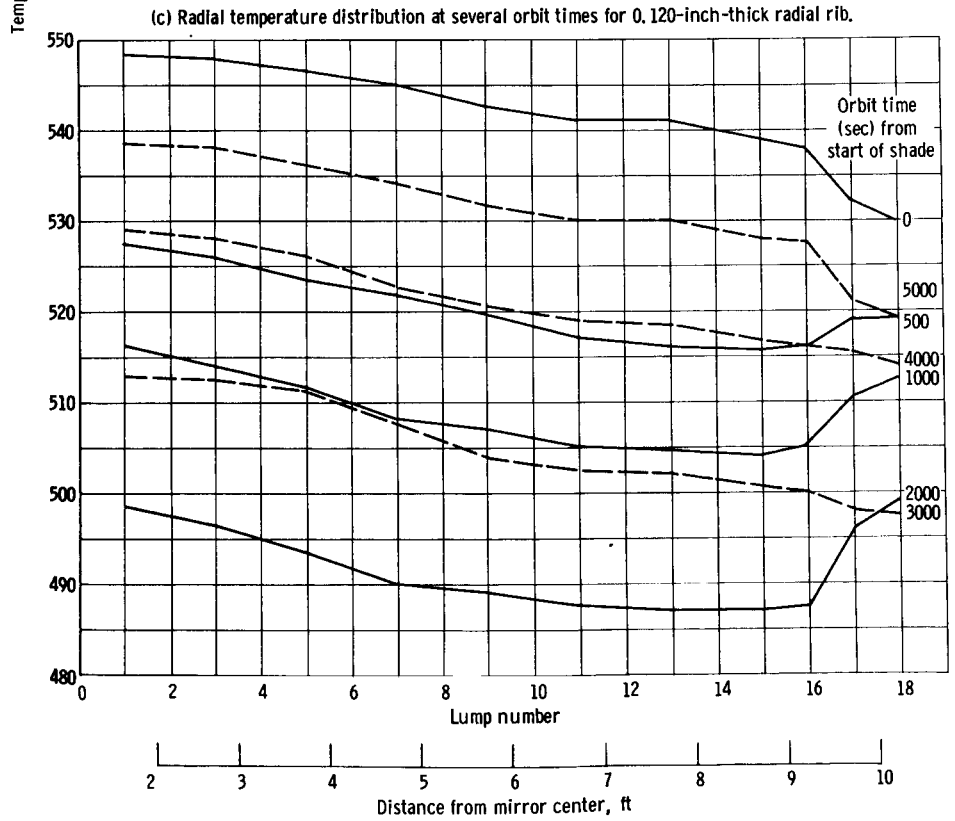

(d) Radial temperature distribution at several orbit times for 0.380-inch-thick radial rib.

Figure 12. - Concluded.

table I, p. 5). As discussed previously, the heat inputs to the collector varied not only with orbit position but also with position along the radial rib.

The temperature variations of several lumps with orbit time for the 0.120-inch rib are shown in figure 12(a). The maximum temperature difference is seen to be the temperature difference between lumps 1 and 18 and is 30° F; this difference exists for about the final 1700 seconds that the collector is in the Sun. The radial temperature distribution can be seen better in figure 12(c) where the variation of temperature with radius is shown for several orbit times. Typical temperature gradients between lumps are about 0.27° F per inch except for the gradient between lumps 16 and 17 that reaches a maximum of 1.3° F per inch at the beginning and end of the shade period. The reason for this increase is because lumps 17 and 18 have extra deep ribs for structural reasons and consequently have a longer thermal lag.

The temperature variations of several lumps with orbit time for the 0.380-inch-thick rib is shown in figure 12(b). The maximum temperature difference was again between the temperatures of lumps 1 and 18 and is about 20° F. This temperature difference

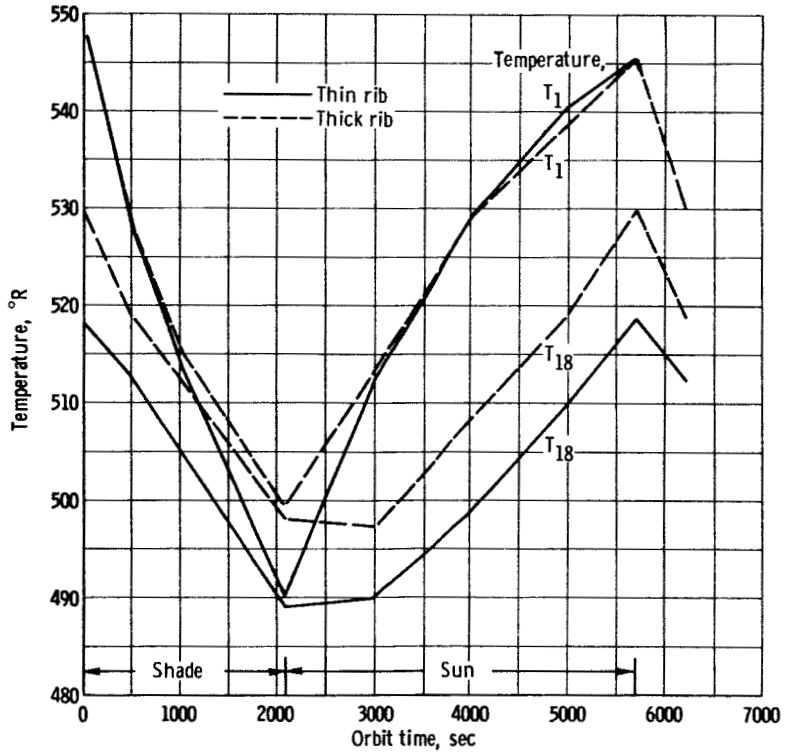

Figure 13. - Comparison of temperatures for 0.120- and 0.380-inch-thick radial ribs for lumps 1 and 18.

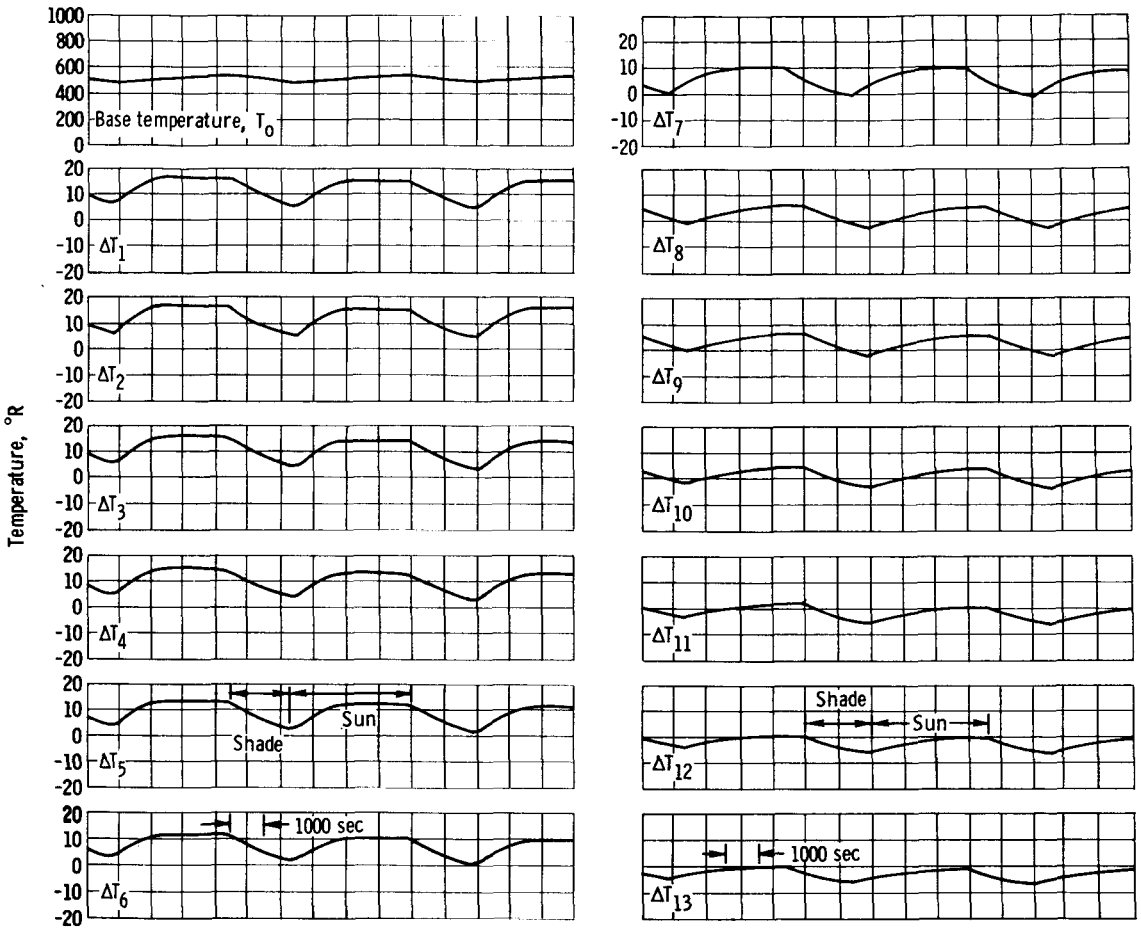

Figure 14. - Time histories of temperatures and heat inputs for the 0.120-inch-thick radial rib.

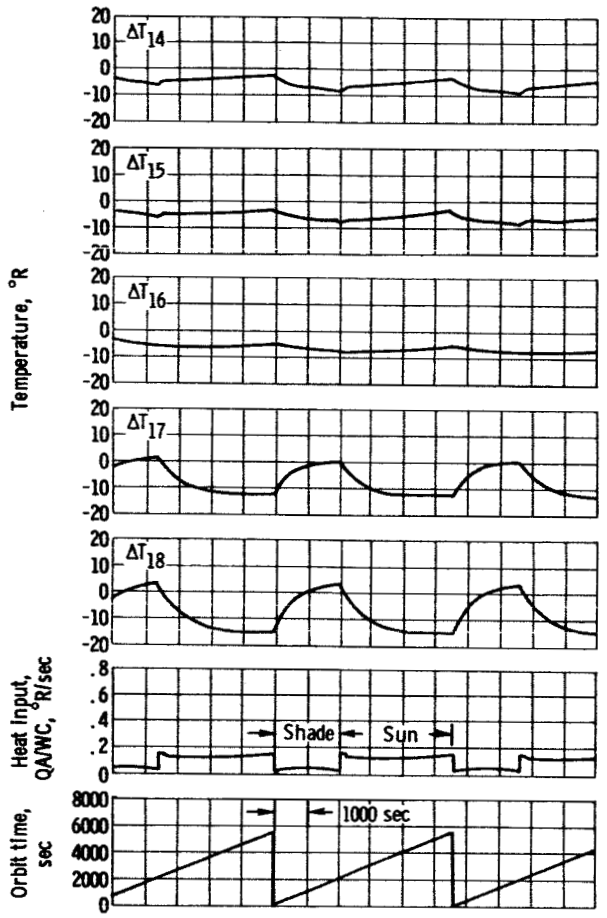

Figure 14. - Concluded.

exists for approximately the last 1700 seconds of each Sun period and is 10° F less than the temperature difference for the 0.120-inch rib study. The radial temperature distribution for various orbit times for the 0.380-inch study is shown in figure 12(d). Typical temperature gradients between lumps are 0.17° F per inch, and the maximum gradient again occurs between lumps 16 and 17; this gradient reaches a maximum of 1.3° per inch.

An estimate of the maximum circumferential gradients that may exist as the collector orbits the Earth was made by comparing the radial temperature distribution of the 0.120- and the 0.380-inch-thick rib (circumferential conduction being neglected). A comparison of the temperatures for lumps 1 and 18 of the two ribs is shown in figure 13 as a function of orbit time. The maximum circumferential temperature differences occur at the end of the shade period, and there are 9° F (0.185° F/in.) between the thick and thin ribs for lump 18 and 8° F (0.925° F/in.) for lump 1. It should be noted that the temperature difference for lump 1 exists only near the end of the shade period and the beginning of the Sun period, while the temperature difference for lump 18 exists during the entire orbit. These temperature differences, however, represent the maximum

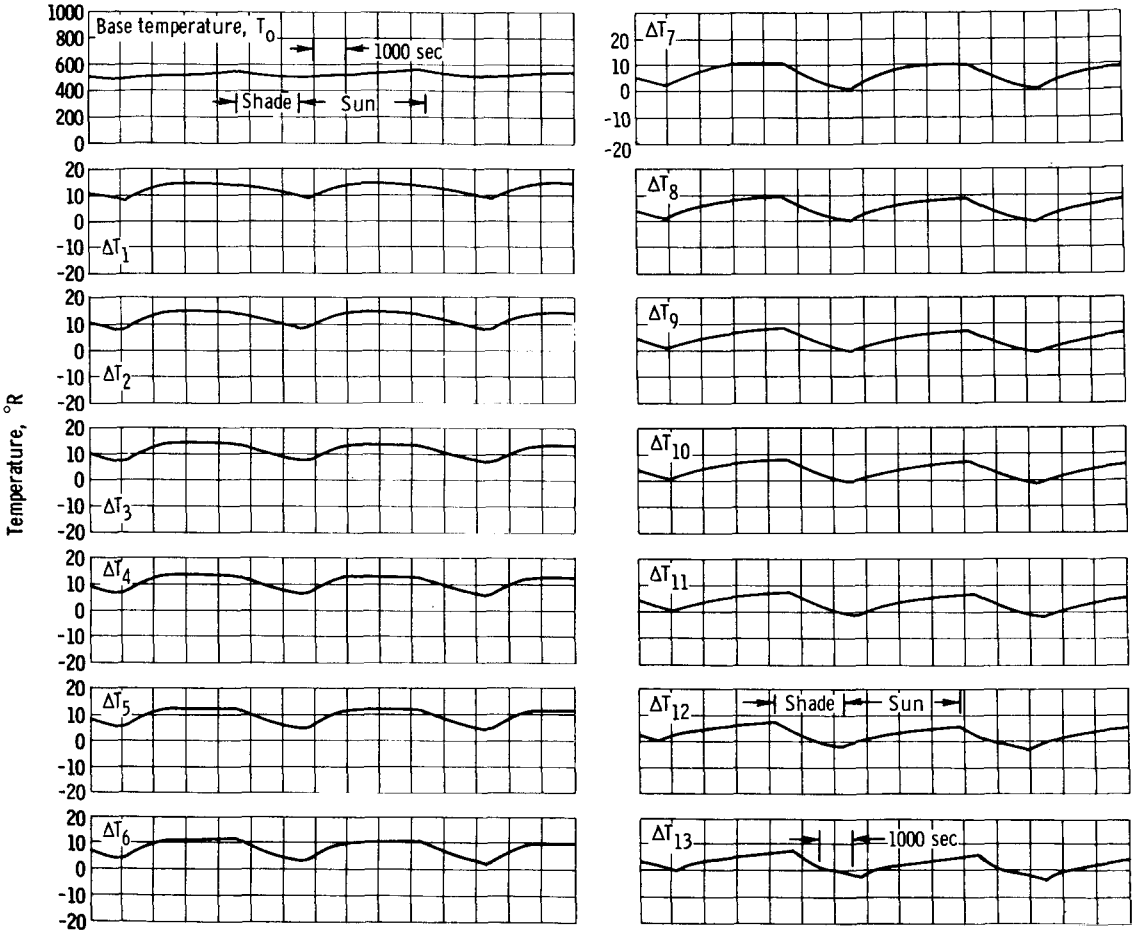

Figure 15. - Time histories of temperature and heat input for the 0.380-inch-thick radial rib.

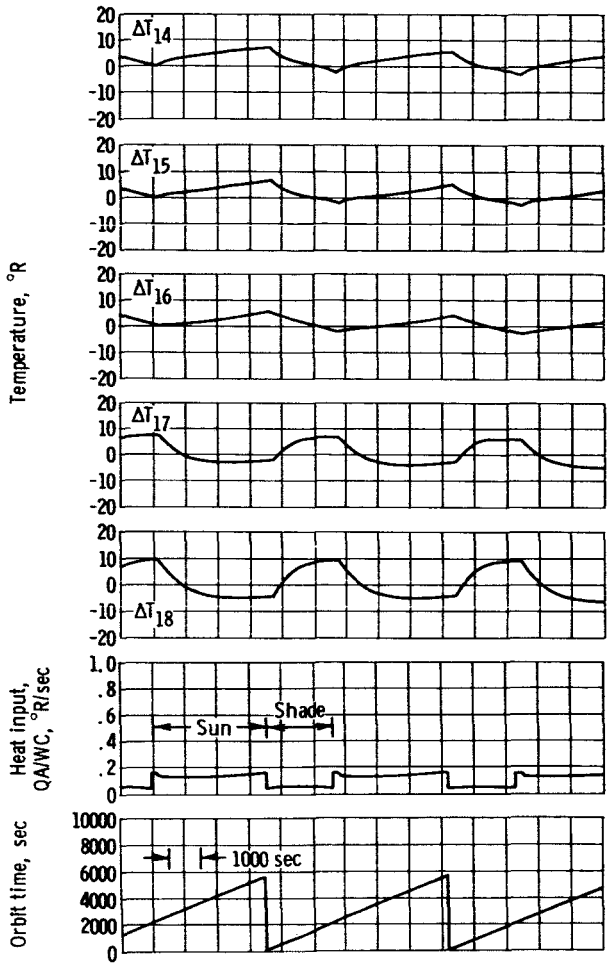

Figure 15. - Concluded.

possible, and actual values will be less because of conduction between the ribs.

Time histories obtained for each of the node perturbation temperatures, approximate average sector temperatures and some of the representative heat inputs are shown in figure 14 for the 0.120-inch-thick radial rib. Similar time histories are presented for the 0.380-inch-thick radial rib in figure 15.

SUMMARY OF RESULTS

The results of the surface section and radial temperature distribution studies can be summarized as follows:

1. The maximum surface and rib temperature gradients during Sun operation occurred shortly after leaving the shade, which resulted in gradients of approximately 0.23° R per inch across the sheet and 0.70° R per inch across the rib. The maximum sheet and rib temperature gradients during an orbit, however, occurred as the collector

left the Sun period. These gradients were up to 50 percent larger than the maximum gradients occurring during the Sun period, but they are not as important because collector distortion during shade operation does not affect power system performance.

2. The results indicate that rib depth is critical in determining the surface temperature gradient: the shorter the rib depth, the less the gradient. Section sizes in the range studied had little effect on the sheet or rib gradients.

3. Of the six combinations of collector surface conditions studied, the two with the back of the collector insulated resulted in the lowest temperature gradients. With the back of the collector insulated, the polished metal front resulted in slightly lower temperature gradients than were obtained with the silicon-oxide coating on the front.

4. The temperature distribution along the 0.120-inch-thick radial rib at the center of the 45° sectors was fairly uniform with a temperature gradient of about 0.27° F per inch. One exception to this uniformity occurred near the outside edge of the collector where the radial rib depth increased from 1.5 to 4.0 inches in 6.0 inches of length. Through this transition the temperature gradient attained a maximum value of 1.3° F per inch at the beginning and end of the shade period.

5. The temperature distribution along the 0.380-inch rib, which forms the boundary between two of the 45° sectors, was fairly uniform with temperature gradients along the rib of about 0.17° F per inch. One exception to this uniformity occurred in the rib transition, as mentioned previously, where the gradient over the 6.0-inch-length-rib was 1.3° F per inch.

6. An estimate of the maximum circumferential gradients that may exist was made by comparing the temperature distributions along the 0.120- and 0.380-inch-thick radial ribs. The maximum circumferential temperature gradient along the outer region of the collector is estimated to be 0.185° F per inch and could exist throughout the entire orbit. The maximum circumferential gradient at the inner portion of the collector is estimated at 0.925° F per inch, but it only exists for a short time near the end of the shade period and beginning of the Sun period.

Lewis Research Center,
National Aeronautics and Space Administration,
Cleveland, Ohio, May 5, 1966,
123-33-04-03-22.

REFERENCES

1. Springer, L. M.: Study, Design, and Fabrication of Solar Energy Concentrator Models. (RTD-TDR-63-4051, DDC No. AD 439838), Electro-Optical Systems, Inc., Apr. 1964.

2. Swanson, P.: Solar Reflector Foaming Technology Development. (AFAPL-TR-64-128, DDC No. AD 609223), Goodyear Aerospace Corp., Dec. 1964.